Event-Based Interferometry for Acoustic Imaging and Signal Reconstruction

Kyra Lee, Bui Le

October 2025

Abstract

This work explores the use of event-based sensing for optical interferometric vibrometry. A Michelson interferometer was constructed with a coherent laser source and a reflective latex membrane serving as the vibrating surface. The interferometric signal was captured using a *DAVIS346* event-based camera, enabling microsecond temporal resolution of optical intensity changes associated with acoustic excitation. To systematically characterize the system's response, we conducted a frequency sweep across nine acoustic frequencies (75–115 Hz) while recording event streams from the interference pattern.

Spatial windowing techniques were applied to isolate regions of maximum event activity, and temporal windowing was performed using both Nyquist-based and global binning strategies. The resulting temporal event distributions revealed clear periodic structure consistent with the applied acoustic frequencies, demonstrating that the event-based sensor successfully encoded the vibration-induced optical modulation.

These findings establish that event-based interferometric imaging can capture low-frequency surface vibrations without requiring high-speed frame-based acquisition. The results highlight the feasibility of using neuromorphic vision sensors for optical vibrometry and motivate future extensions toward real-time frequency reconstruction and event-domain noise characterization.

I. Introduction

Laser interferometry is a powerful optical technique that extracts quantitative information from the interference of coherent light waves. It has long been used for high-precision measurements of displacement, vibration, and surface motion in scientific and engineering applications [1, 2, 3, 4] One common implementation is the laser vibrometer, which measures surface vibrations by comparing the laser light reflected from the target surface with a reference beam. When these two beams recombine at the sensor, their interference pattern encodes the phase variations caused by the surface motion, enabling accurate estimation of vibration amplitude and frequency.

Among existing optical vibrometry techniques, interferometric methods such as Michelson interferometry are widely used due to their ability to measure nanometer-scale displacements with high precision [5, 6]. These systems rely on the interference between a reference and a reflected beam, where the resulting fringe patterns encode surface motion (Fig. 1). However, traditional frame-based implementations of interferometric vibrometers are constrained by the speed and cost of high-frame-rate cameras. Capturing high-frequency vibrations requires rapid frame acquisition, which generates massive data volumes, increases latency, and introduces computational bottlenecks in post-processing [8, 9].

To overcome these limitations, we explore the use of event-based cameras for optical interferometry. Event-based sensors record changes in logarithmic intensity asynchronously at the pixel level, providing microsecond temporal precision, high dynamic range, and dramatically reduced data throughput compared to conventional imaging sensors [7, 10, 13] These properties make event cameras particularly suited for measuring dynamic optical signals, where rapid variations in interference fringes occur due to surface vibrations.

Previous research has explored the usage of event cameras for optical vibration sensing, most notably in the Event2Audio framework developed by Cai et al [7]. In their work, event-based cameras were employed to recover audio signals underwater, and the primary focus was on achieving high-quality reconstruction of sound as a proof-of-concept for event-based vibrometry. In contrast, our work does not aim to reconstruct audio signals

but instead investigates the feasibility of using an event-based camera within a Michelson interferometric setup to measure the temporal and spatial dynamics of surface vibrations at known frequencies. By leveraging interferometry, we encode vibration information into interference patterns captured by the event camera, allowing us to analyze event accumulation, temporal distributions, and frequency-domain characteristics. This approach emphasizes quantitative characterization of vibrational responses rather than audio reconstruction, providing complementary insight into the application of event cameras for optical vibrometry in controlled experimental conditions.

In this work, we investigate the feasibility of using an event-based camera as a sensing element in a Michelson interferometer to measure vibration frequencies of a reflective surface. By illuminating a surface with coherent light and analyzing the resulting interference signal through the event stream, we aim to capture both the temporal and spatial dynamics of the vibration. The proposed setup maintains a simple and compact optical design while leveraging the inherent speed and efficiency of event-based sensing.

Our key goals are as follows:

- To develop an event-based Michelson interferometric system capable of capturing vibration-induced interference patterns with high temporal precision.
- To demonstrate the ability of the event camera to record distinct vibration frequencies within the 75–115 Hz range, highlighting its sensitivity to optical phase variations.
- To evaluate the recorded event data and explore event accumulation and frequency-domain analysis as a pathway toward event-based optical vibrometry.

Overall, this work represents an early step toward real-time event-based interferometric sensing, demonstrating its potential for precise, high-speed measurement of dynamic surface motion.

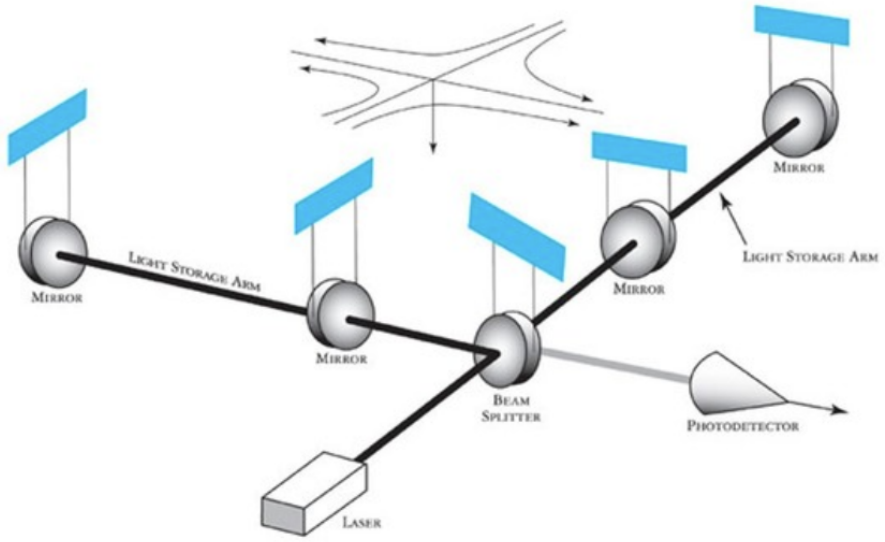

Figure 1: *Standard Michelson interferometry setup*

II. Theoretical Background

The basic theory of the Michelson interferometer is discussed in the this section. Essentially, the subtle motion of reflective surfaces can be measured with precision using optical interferometry, which converts nanoscale displacements into measurable interference patterns of coherent light. Specifically, when two beams—one reflected from a vibrating surface and the other from a fixed reference mirror—recombine, their relative phase encodes the surface's motion as a measurable intensity modulation at the detector. In a Michelson configuration, this interference pattern can be expressed as

$$I(t) = I_0 \left[1 + \cos\left(\frac{4\pi}{\lambda}\Delta z(t)\right)\right],$$

where I_0 is the mean intensity, λ is the wavelength of the laser, and $\Delta z(t)$ is the instantaneous displacement of the reflective surface. Variations in the surface position therefore produce time-varying intensity fringes, whose

temporal oscillations correspond directly to the vibration frequency of the surface, which has been shown by Fu et al [11]. These principles have long underpinned traditional laser vibrometry systems, which are capable of resolving extremely small displacements by tracking the phase evolution of interference fringes.

However, conventional interferometric vibrometers typically rely on frame-based cameras, which capture sequences of images at fixed frame rates. The temporal resolution of such systems is limited by the maximum frame rate and exposure time, leading to a trade-off between measurement accuracy, data volume, and computational cost [8]. Capturing fast or high-frequency vibrations requires frame rates that are both technologically demanding and data-intensive, constraining real-time or continuous monitoring applications. Event-based cameras, by contrast, offer a fundamentally different sensing paradigm. Instead of recording full image frames, these neuromorphic sensors asynchronously detect changes in logarithmic intensity at the pixel level. Each pixel triggers an ON or OFF event when the change in log-intensity $\Delta \log I$ exceeds a contrast threshold C, such that

$$\Delta \log I > C.$$

This design allows for microsecond-level temporal precision, high dynamic range, and dramatically reduced data throughput compared to traditional sensors [10, 13]. When integrated into an interferometric setup, the dynamic interference fringes generated by a vibrating surface translate directly into asynchronous streams of ON and OFF events that trace the temporal evolution of the optical phase. In this context, the temporal density of events reflects the frequency and amplitude of the underlying vibration. Rapid phase modulations in the interference pattern produce higher event rates, while slower oscillations yield more sparsely distributed activity. By aggregating these events over time to reconstruct an approximate signal $s(t)$, it becomes possible to analyze the temporal frequency content of the surface motion using Fast Fourier Transform (FFT) techniques. This process effectively bridges optical interferometry and event-based sensing: surface motion is transduced into phase variations, encoded as intensity modulations, and finally discretized into event streams from which vibration frequencies can be recovered.

The theoretical basis presented here establishes the foundation for the subsequent mathematical and analytical framework. The following section formalizes this relationship between optical phase variation and event generation, providing the groundwork for the experimental design and subsequent analyses of event-based interferometric signals.

III. Preliminary Mathematics

To model the underlying optical principles of our interferometric setup, we first consider the acoustic vibrations of a reflective surface—specifically, a stretched latex glove—measured using a Michelson interferometer with a laser wavelength of $\lambda = 600\,\text{nm}$. The surface vibration amplitude Δx induces a phase shift in the reflected beam, causing the interference pattern at the sensor to modulate. When the reflective surface moves by Δx, the optical path length from the laser to the sensor changes by $2\Delta x$, and the the resulting phase shift is as follow:

$$\Delta\phi = \frac{4\pi\Delta x}{\lambda}$$

where:

- $\Delta\phi$ is the phase change in radians
- Δx is the surface displacement
- λ is the laser wavelength (600 nm)

We can define the complex fields returning to the detector from the two beams be $U_1 = A_1 e^{j\phi_1}, U_2 = A_2 e^{j\phi_2}$, where $A_1 = \sqrt{I_1}, A_2 = \sqrt{I_2}$, and I_1, I_2 are the intensities the arms would deliver when the other arm is blocked. The total field is:

$$U = U_1 + U_2$$

Then, the intensity of light at any point in this complex scalar field can be calculated using the principle of interference[12]:

$$I = I_1 + I_2 + 2\sqrt{I_1 I_2}\cos(\Delta\phi)$$

where:

- I_1 = reference arm intensity
- I_2 = signal arm intensity (reflected from vibrating surface)

- $\Delta\phi = \phi_2 - \phi_1$

Let us assume a perfect environment where there is no light absorbtion and environmental interference. Then, we can assume that $I_1 \approx I_2$ as the two beams originated from the same laser, which makes the combined intensity of the beams be:

$$I = 4I_o cos^2(\frac{\Delta\phi}{2})$$

To maximise the events generated by the phase difference, the initial phase difference should be $\Delta\phi = k\pi$ (destructive interference). Then, a sound wave is introduced to shift the phase by π radian so that $\Delta\phi = 2k\pi$, resulting in constructive interference. This would cause the combine intensity to go from I_{min} to I_{max}, maximising the probability of generating an event.

One full fringe shift in intensity period in a Michelson interferometer corresponds to a surface displacement of:

$$\Delta x_{fringe} = \frac{\lambda}{2} = 300\,\text{nm}$$

For a phase change of $\Delta\phi = 1$ radian, the required surface displacement is:

$$\Delta x = \frac{\lambda}{4\pi} \approx \frac{600 \times 10^{-9}}{4\pi} \approx 47.7\,\text{nm}$$

A phase change of $\Delta\phi = 1$ radian would cause a change of approximately 23 percent. Under the default bias conditions of the *DAVIS346* sensor and in a controlled dark environment, this intensity variation is sufficient to trigger an event.

While a theoretical estimate of the expected acoustic vibration amplitude is provided in Appendix A, in practice, precise modeling of material elasticity and acoustic coupling exceeds the scope of this project. Instead, we performed a controlled frequency sweep—spanning 75 Hz to 115 Hz at constant amplitude—to empirically determine the frequencies that most effectively modulate the interferometric signal and elicit event responses.

IV. Data Collection

Overall Experimental Design

The experimental data were acquired using a Michelson interferometric setup designed to capture acoustic surface vibrations through event-based sensing. The setup consisted of a coherent laser source with a wavelength of $\lambda = 600$ nm, which was split into reference and measurement arms using a beam splitter. The measurement arm was directed toward a reflective surface composed of a stretched latex glove, which served as the vibration medium. Acoustic excitation was provided by a calibrated speaker positioned near the latex, driven at controlled sinusoidal frequencies within the audible range (Fig. 2).

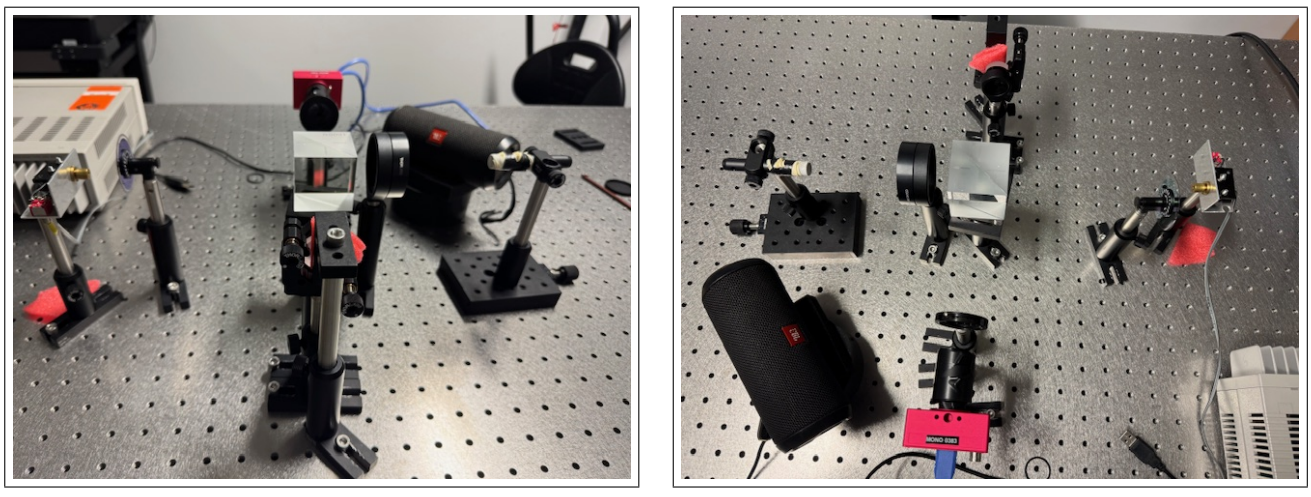

Figure 2: *Two viewpoints of the experimental interferometry setup showing the laser, latex surface, and DAVIS346 sensor. Photographs were taken under normal lighting without the cardboard box for clarity.*

The surface vibrations induced by the acoustic pressure modulated the optical path length of the reflected laser beam, producing interference fringes when recombined with the reference beam. These interference patterns were recorded using a *DAVIS346* event-based camera, which asynchronously detects changes in light intensity at the pixel level. Unlike conventional frame-based cameras, the DAVIS sensor outputs events corresponding to brightness changes over time, enabling microsecond-level temporal resolution and high dynamic range.

Each experimental trial corresponded to a specific modulation frequency emitted by the speaker. For each frequency, event data were recorded for several seconds to ensure sufficient sampling of the steady-state vibration pattern. In addition, to minimize external disturbances, a cardboard box was placed over the sensor and laser beams, and all measurements were performed in a dark and silent environment. This ensured that only vibrations of the latex surface induced by the controlled acoustic signal were recorded. The resulting event streams were stored as text-based files containing timestamped events of the form (t, x, y, p), where t denotes the event timestamp (in microseconds), (x, y) are the pixel coordinates, and p encoded as binary values, with 1 representing ON events and 0 representing OFF events. Furthermore, baseline measurements were acquired under two static conditions: (1) with the laser pointed at the center of the latex glove in the absence of speaker excitation, and (2) with the laser directed at the edge of the metallic apparatus to verify negligible mechanical vibrations.

Equipment Parameters

The optical path lengths and key distances of the interferometric setup were as follows:

Component	**Distance**
Beam splitter → cube center	10 cm
Lens → box	39.5 cm
Lens → cube center	5 cm
Lens → camera	9 cm
Camera → optical filter	15.5 cm
Filter → cube center	9.5 cm
Camera → cube center	5.5 cm
Box → far mirror	34 cm
Far mirror → lens	74 cm

Table 1: *Key distances in the event-based interferometry setup.*

These distances ensured proper alignment of the reference and measurement beams, as well as optimal focusing on the reflective latex surface. Together, the surface vibrations induced by the acoustic pressure modulated the optical path length of the reflected beam, producing interference fringes when recombined with the reference beam. Acoustic excitation was applied using a calibrated speaker positioned at a set distance from the latex surface. For each frequency, the speaker amplitude was controlled at a constant sound pressure level to ensure repeatable excitation. Each experimental trial corresponded to a specific modulation frequency emitted by the speaker.

Trials and Repetitions

For each frequency, two independent trials were recorded, each lasting approximately five seconds to ensure adequate sampling of the vibrational patterns. A single latex glove was used for all measurements to maintain consistency, and the experimental setup remained fixed between trials. The latex glove was chosen as the vibratory surface because it responded primarily to lower-frequency acoustic inputs. To systematically characterize the sensor response, a frequency sweep was performed across nine acoustic frequencies: 75, 80, 85, 90, 95, 100, 105, 110, and 115 Hz. This procedure enabled comprehensive capture of both the temporal and spatial dynamics of event activity across the relevant vibrational range.

V. Results

In this section, we present a comprehensive overview of the pre-processed event-based interferometry data across all tested acoustic frequencies. The analysis encompasses both spatial and temporal dimensions of the recorded events, providing a multi-faceted perspective on the sensor's response characteristics. Spatially, we employ a windowing approach to identify regions of maximal event density within the area of interest. These high-activity regions are subsequently mapped across different frequency bands, allowing for a detailed examination of how localized sensor responses vary under distinct acoustic modulations (Fig. 3). This approach not only reveals

the spatial distribution of sensitivity across the sensor surface but also highlights potential inhomogeneities or localized enhancements in response amplitude.

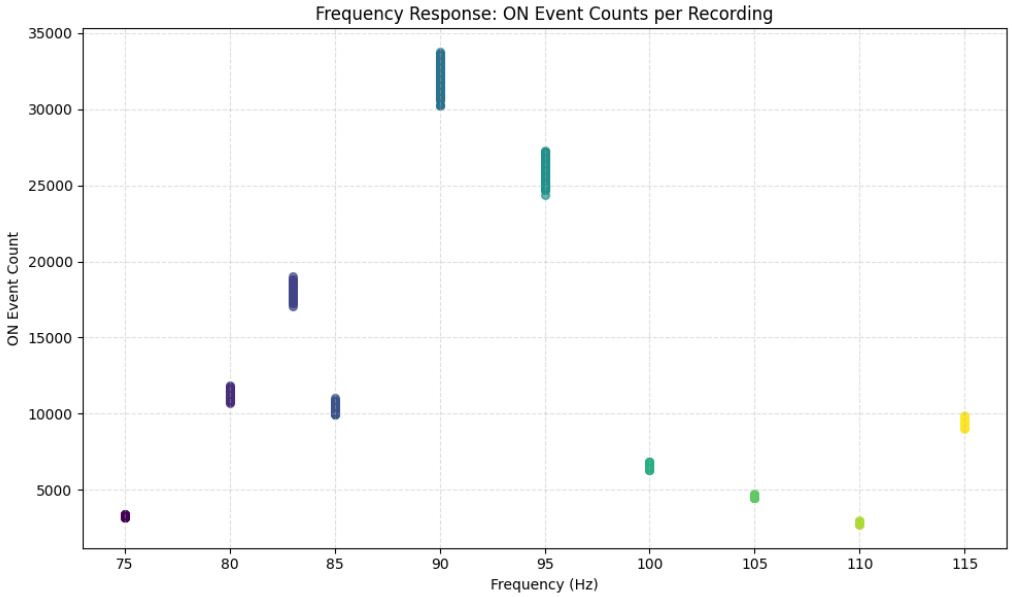

Figure 3: *Total ON event counts per region of interest (ROI) across all frequencies, scaled to one dot per thousand events.*

Temporally, we quantify the frequency of event occurrences within each bin, both under a uniform global binning strategy and a Nyquist-based temporal window, enabling an evaluation of event dynamics over time. The temporal distributions are further analyzed using Fast Fourier Transform (FFT) computations, which facilitate the identification of dominant frequencies present in the sensor outputs. The FFT spectra allowed us to directly compare the sensor's temporal responses against the known input frequencies, validating both the detection accuracy and temporal resolution of the event-based sensor. Notably, in all cases, multiple peaks were observed in the spectra, likely corresponding to harmonics of the stimulus since peaks occurred at integer multiples of the fundamental frequency.

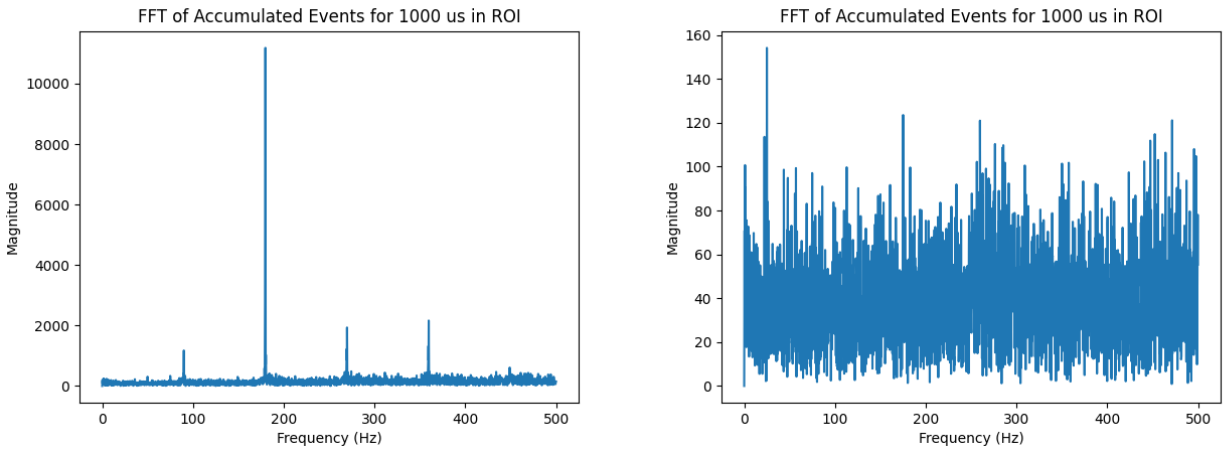

Figure 4: *FFT analysis comparing the sensor's response to the 90 Hz stimulus (left image) versus the baseline frequency which had no additional stimulus (right image).*

This multi-dimensional approach of spatial and temporal analysis not only highlights the consistency and amplitude of the sensor's response but also enables the identification of key temporal and spatial patterns across frequencies. By correlating these patterns with the frequency-specific behavior, we gain a deeper understanding of how the sensor reacts to acoustic modulations at different scales.

VI. Analysis Process

0.1 Raw Events to Event Accumulation

Prior to any accumulation or processing, the recorded data consisted of raw neuromorphic events directly output by the *DAVIS346* event-based camera. Each event represents a localized change in light intensity at a specific pixel and timestamp, encoded in the form (t, x, y, p). Figure 5 illustrates a sample of raw events captured during a single experimental trial. In this visualization, individual events are plotted, but due to the asynchronous and sparse nature of event-based sensing, only pixels experiencing brightness changes generate events. However, raw event streams are inherently noisy, with spurious events arising from sensor noise, background light fluctuations, or minor uncontrolled vibrations. This noise can obscure subtle patterns in the interference fringes and makes direct interpretation of the raw events challenging. Despite this, these raw event streams serve as the fundamental data for all subsequent analysis, including accumulation, filtering, and Fourier-based transformations, where noise can be mitigated and meaningful patterns extracted.

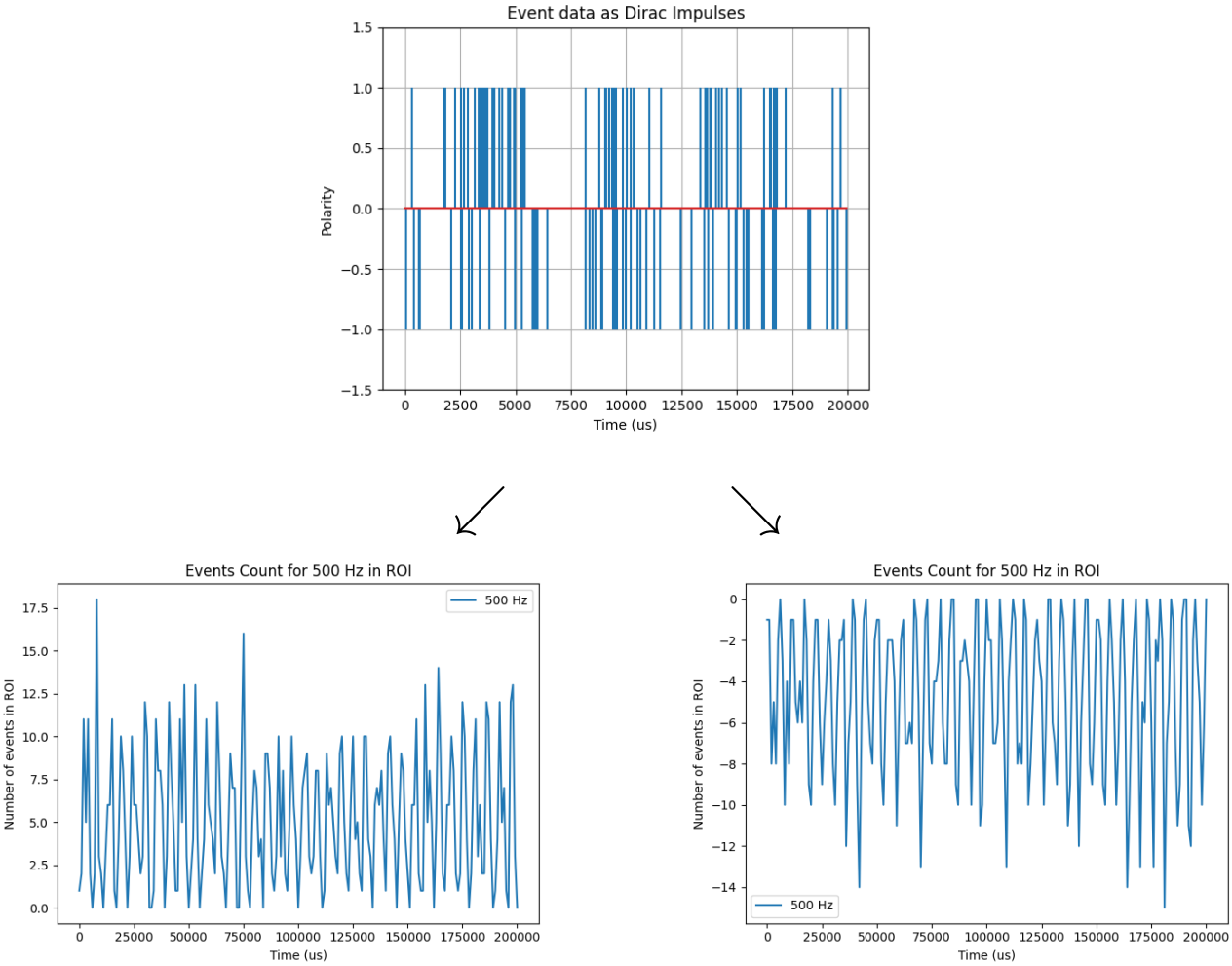

Figure 5: *Raw event spikes subsequently accumulated and separated into ON (left) and OFF (right) events.*

Thus, event pre-processing began by accumulating ON, OFF, and ON + OFF events. However, the initial accumulation revealed significant noise in the global environment, which prompted the implementation of both spatial and temporal windowing techniques. Spatial windowing helped focus analysis on specific regions of interest, minimizing the influence of peripheral noise, while temporal windowing ensured that only relevant event windows were considered, reducing artifacts caused by transient or irrelevant activity. This approach significantly improved the accuracy of the analysis by reducing noise, eliminating hot pixels, and ensuring that only the most relevant event data were retained for further analysis.

0.2 Spatial Windowing for Event Distributions

To identify regions of maximal event activity within the sensor's field of view, we employed a spatial windowing approach. First, heatmaps of the ON, OFF, and ON + OFF events were generated for each frequency (Fig. 6 shows all heatmaps for 90 Hz). In these heatmaps, "ON" and "OFF" events refer to specific polarities of the events, while "ON + OFF" combines both. Next, a small square window of 10 x 10 pixels was systematically moved across the entire event heatmap, and the total number of ON, OFF, and ON + OFF events within each window position was computed. The window location with the highest accumulated event count was selected as the region of interest (ROI), capturing the area of the sensor with the most significant activity. This window was then zoomed in for visualization, providing a clear depiction of the localized spatial distribution of events (Fig. 7 shows all ON events for each frequency's ROI).

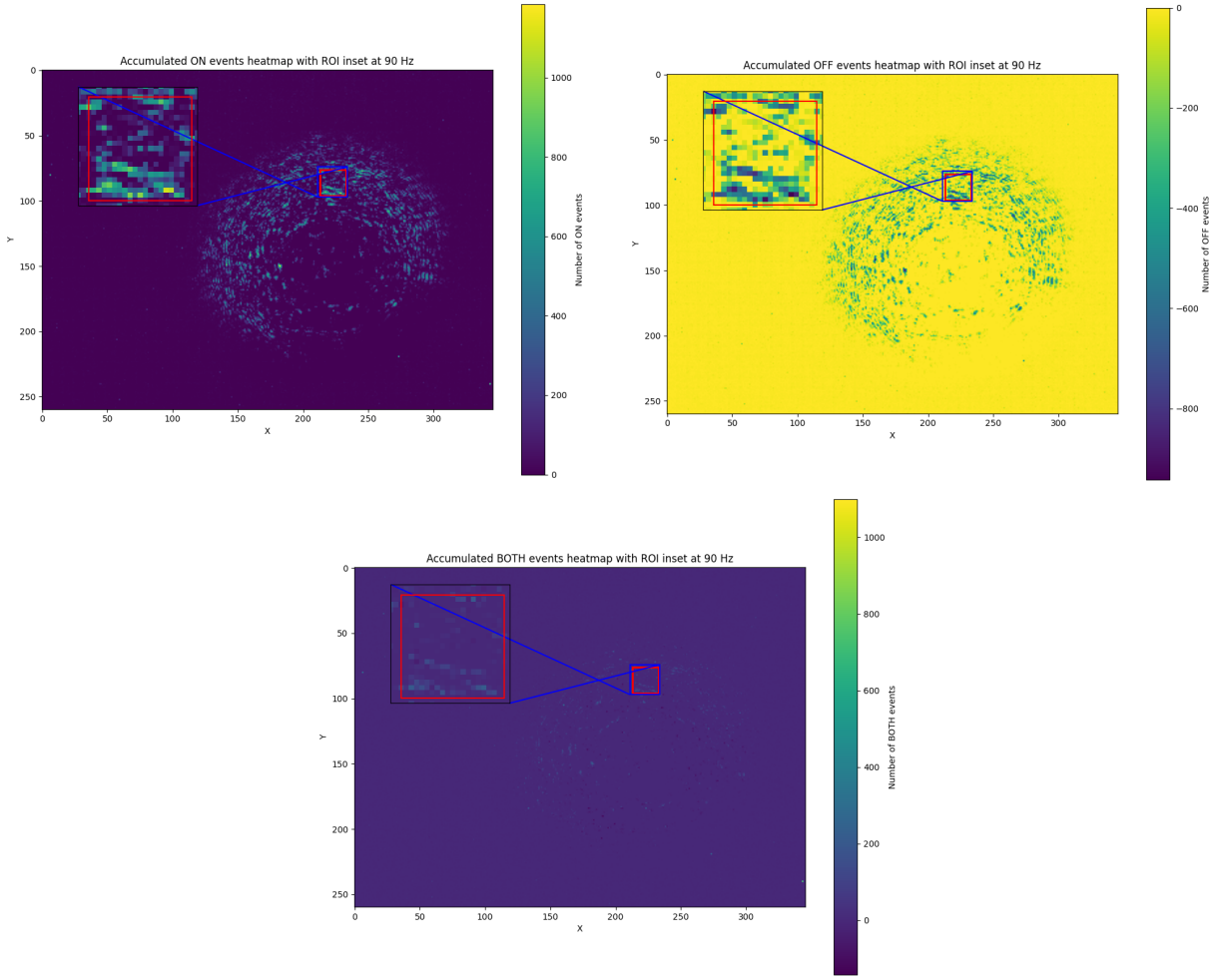

Figure 6: *Zoomed in 10 x 10 spatial window of maximum event activity within the ROI.*

By focusing on the ROI, this method ensures that subsequent temporal analyses prioritize the portion of the sensor exhibiting the strongest response to the stimulus. This approach was applied to all frequency data files, ensuring consistency across analyses.

0.3 Temporal Windowing for Event Distributions

For temporal analysis, two complementary windowing strategies were employed to facilitate frequency-domain characterization of the sensor response. First, a Nyquist-based approach was applied, where the time bin size was set to half the period of the stimulus frequency. This ensured sufficient temporal resolution to capture the modulation of the input signal while satisfying the Nyquist criterion, allowing accurate reconstruction of the fundamental frequency components using Fourier analysis. Second, a uniform global window of 1000 µs time-steps was implemented, providing a consistent binning scheme across all frequencies. This approach enabled straightforward comparison of temporal event distributions between stimuli and laid the groundwork for future analyses, such as evaluating trends in event counts and assessing sensor response consistency over time.

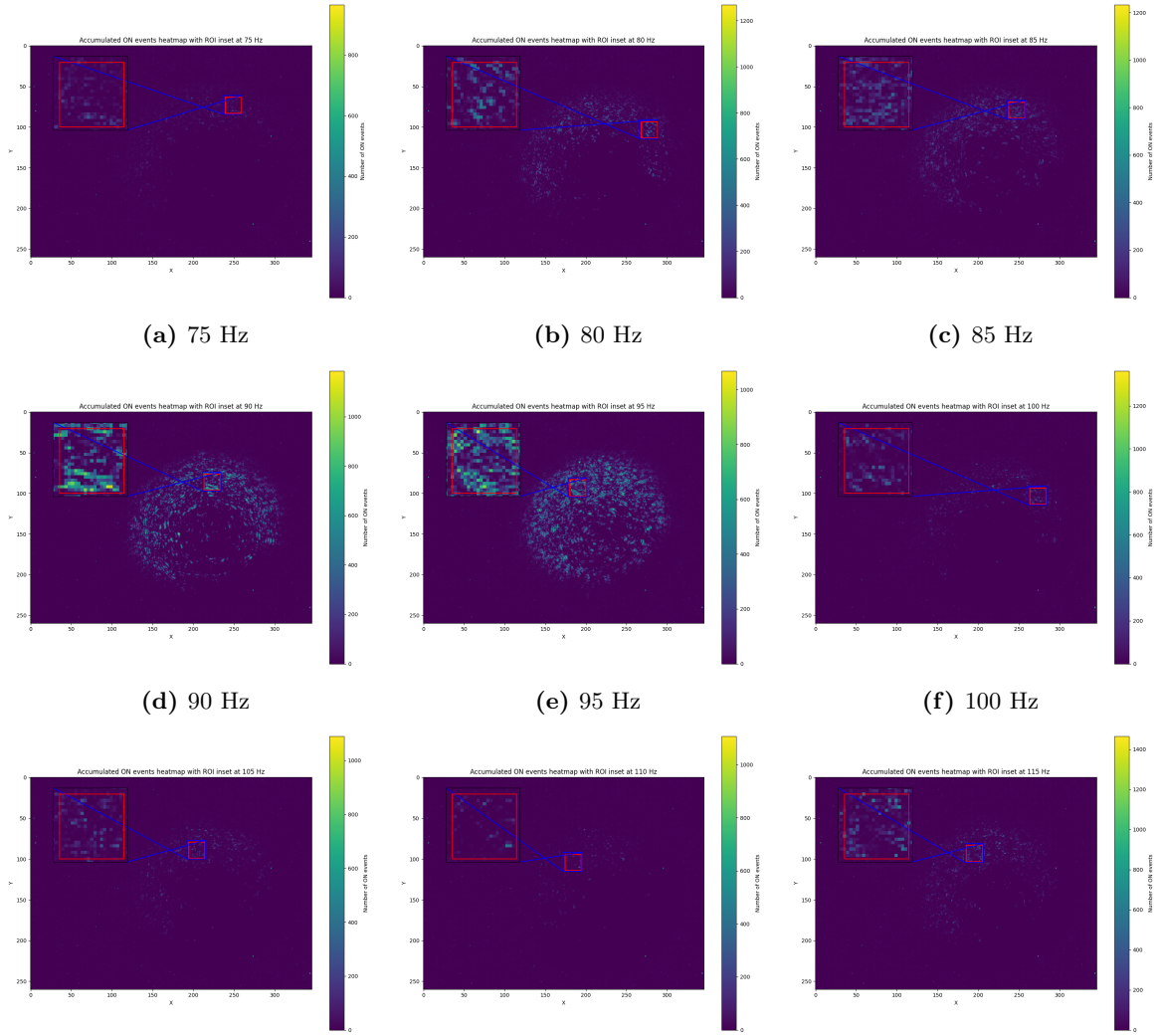

(a) 75 Hz **(b)** 80 Hz **(c)** 85 Hz

(d) 90 Hz **(e)** 95 Hz **(f)** 100 Hz

(g) 105 Hz **(h)** 110 Hz **(i)** 115 Hz

Figure 7: *Spatially windowed ROIs with the highest ON activity across different frequency bands.*

Figures 8 and 9 summarize the temporal characteristics of ON event activity across all tested frequencies. Figure 8 presents the mean and standard deviation of temporal ON event counts per bin, computed using the uniform global window. These distributions provide a detailed view of how event activity evolves over time within the selected region of interest (ROI), highlighting both the consistency and variability of sensor responses under different acoustic stimuli. Figure 9 complements this analysis by displaying the total number of ON events detected for each frequency using the same uniform global window. This plot offers a high-level overview of overall sensor activity, facilitating direct comparison of relative signal strength across the tested acoustic inputs. Together, these figures provide a comprehensive depiction of the temporal event distributions, illustrating both fine-grained temporal behavior and aggregate sensor response across frequencies. Further spectral analysis via FFT also did confirm the harmonic relationships by demonstrating peaks at integer multiples of the fundamental stimulus frequency, strengthening the interpretation of these recurring temporal features.

0.4 FFT Analysis Process

Fourier Transforms are one of the most widely used family of algorithms in signal analysis and other mathematical fields. It transforms a signal into its frequency components, allowing the identification of the frequencies present in the original signal as well as the strength of each frequency[16]. This is particulary useful for this project as it is the main tool used to identify the frequency of the reflected laser beam.

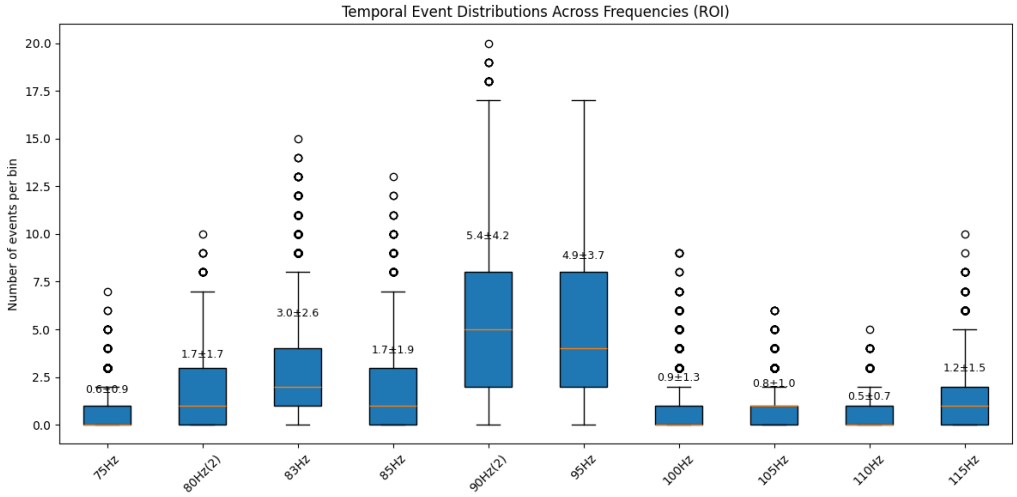

Figure 8: *Mean and standard deviation of all ON temporal event counts per global temporal bin across frequencies in the selected ROI.*

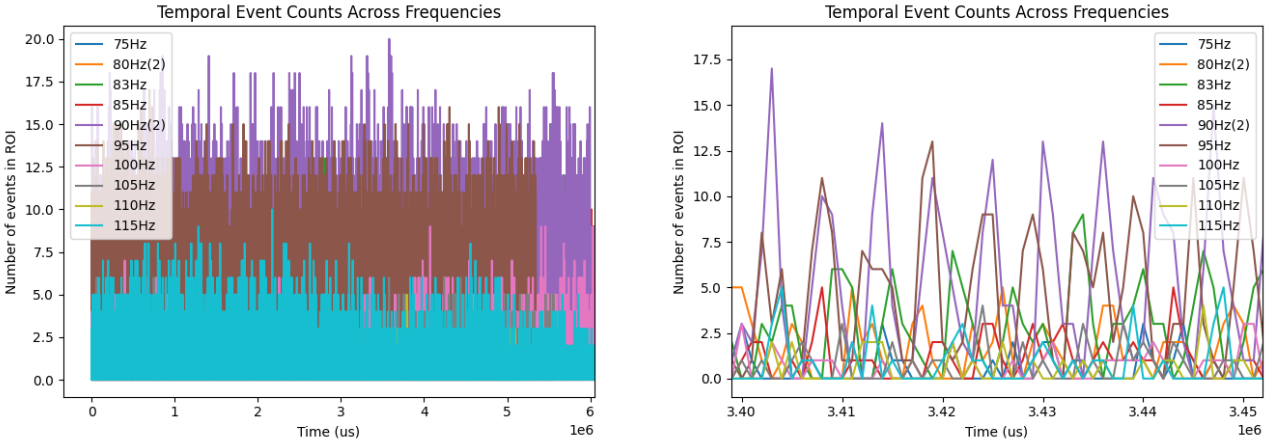

Figure 9: *Total ON events per frequency in the selected ROI using the uniform global window shown both zoomed out and zoomed in.*

Following data preprocessing, a preliminary Fourier analysis was performed to assess whether meaningful spectral information could be extracted from the event data. To prepare the data for the Discrete Fourier Transform (DFT), event timestamps were first divided into uniform temporal bins using a Nyquist-based approach. This step effectively converts the nonuniform event stream into uniformly sampled data suitable for FFT computation.

The resulting Figure 10 shows that even with spatial windowing, the nosie is still significant. However, a substantial magnitude near 90 Hz shows that the dominant frequency for this analysis is very close to 90 Hz. This is consistent with our data as this analysis was done on the data file recording the experiment with sound playing at 90 Hz.

It is important to note that this plot does not display the complete frequency response, as the spectrum is truncated at 90 Hz. To further investigate the higher-frequency content, the analysis was extended to a sampling rate of 500 Hz (corresponding to a temporal bin width of 1000 μs). The resulting spectrum, shown in Figure 4, reveals additional peaks near 180 Hz, 270 Hz, and 360 Hz—integer multiples of the fundamental 90 Hz frequency. These harmonics likely originate from nonlinearities or resonant coupling in the vibrating surface or optical setup.

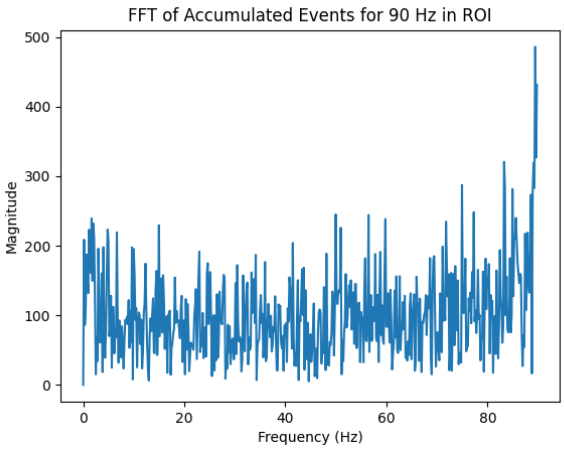

Figure 10: Fourier Transform of the ON events count in the ROI at 90Hz

VII. Discussion

In this study, we employed event-based imaging with the DAVIS346 sensor to capture acoustic vibrations of a latex surface using a Michelson interferometric setup. Our results demonstrate that the temporal event distributions and cumulative event counts vary consistently with the frequency of the acoustic input, indicating that the sensor and setup are sensitive to the intended modulation. These findings are consistent with previous research demonstrating that event-based sensors can capture high-frequency motion with microsecond resolution [7].

The spatial windowing methodology allowed us to isolate regions of maximum ON activity within the region of interest, providing a consistent basis for additional temporal analysis. Similar approaches to isolate regions of maximal activity have been shown to enhance signal fidelity in event-based optical measurements [14]. By applying both global uniform binning and Nyquist-based binning strategies, we were able to capture fine temporal details for FFT analysis while also retaining sufficient resolution for noise characterization. The use of Nyquist-based binning follows established principles for avoiding aliasing in temporally sampled data streams [15], while uniform global binning provides a robust estimate of overall activity, consistent with previous event-based vibration work [7].

Despite these successes, several limitations remain. First, one limitation observed in this study pertains to the temporal binning procedure. Specifically, edge effects in temporal binning have been previously documented in discrete-time signal analysis, where partial data at boundaries can bias statistical estimates [16]. While these effects do not qualitatively change the observed trends across frequencies, they may introduce small quantitative discrepancies in the precise characterization of event activity, particularly in short recordings or when using fine temporal resolution. Second, our ROI selection, while systematic, may not capture all relevant spatial dynamics, and cumulative event counts alone do not fully disentangle signal from noise contributions. Moreover, the sensitivity and noise characteristics of event cameras are inherently influenced by their internal bias settings, which determine how readily the sensor responds to changes in light intensity. In our system, all experiments were conducted using the default bias configuration provided by the manufacturer. Adjusting these parameters could allow finer control over the event generation threshold, enabling improved sensitivity to subtle speckle motion and a higher signal-to-noise ratio. Such optimization would likely lead to more reliable event detection and enhanced spatio-temporal analysis in future experiments.

Future work will aim to address these limitations. Improved FFT analysis could employ adaptive binning or advanced interpolation techniques to better resolve high-frequency components. Pixel-level frequency analysis and repeated trials could enable more precise signal-to-noise ratio (SNR) estimation and temporal mismatch characterization. Furthermore, automated ROI selection and real-time event processing could enhance the accuracy and throughput of measurements, facilitating more detailed mapping of spatial and temporal dynamics.

Overall, this study demonstrates the potential of event-based interferometric imaging for high-resolution spatiotemporal measurements while highlighting opportunities to optimize temporal resolution and noise characterization in future experiments. Our findings suggest that event-based interferometric imaging is a promising tool for capturing dynamic surface vibrations and could be extended to more complex vibrational analyses, with future directions including automated ROI selection, real-time frequency tracking, and advanced noise

reduction techniques.

VIII. Conclusion

In this work, we demonstrated the feasibility of using event-based sensing for optical vibrometry through a Michelson interferometric setup combined with a *DAVIS346* event-based camera. By illuminating a latex membrane with a coherent laser and applying acoustic excitations between 75–115 Hz, we captured temporally precise event streams encoding the surface's vibration dynamics.

Through systematic spatial and temporal windowing, we identified regions of maximum activity and characterized temporal event distributions across frequencies. The results showed consistent modulation patterns aligned with the stimulus frequencies, confirming that the interferometric signal was accurately encoded into the event domain. The use of both Nyquist-based and global temporal binning enabled the preservation of frequency-specific information while supporting broader comparisons of temporal activity.

While this study focused primarily on preprocessing and Fourier-based temporal analysis, the results establish a foundation for more advanced event-domain spectral and noise analyses. Future work will extend this framework to incorporate adaptive temporal sampling, non-uniform fast Fourier transforms (NUFFT) for improved frequency reconstruction under sparse sampling, and systematic noise characterization to quantify sensor stability and signal-to-noise ratios across trials.

Overall, this research demonstrates that event-based interferometric imaging can effectively capture low-frequency vibrations with high temporal resolution, low data throughput, and strong potential for real-time, high-fidelity optical vibrometry applications.

References

[1] Barker LM, Hollenbach RE. Laser interferometer for measuring high velocities of any reflecting surface. *Journal of Applied Physics*: 43, 4669–4675. 1972.

[2] Abbott BP, et al. LIGO: the Laser Interferometer Gravitational-Wave Observatory. *Reports on Progress in Physics*: 72. 2009.

[3] Zhang QM, et al. Laser interferometer for the study of piezoelectric and electrostrictive strains. *Journal of Applied Physics*: 63(8), 2492–2496. 1988.

[4] Smeets G. Laser Interferometer for High Sensitivity Measurements on Transient Phase Objects. *IEEE Transactions on Aerospace and Electronic Systems*: 8(2), 186-190. 1972.

[5] Lawall J, Kessler E. Michelson interferometry with 10 pm accuracy. *Review of Scientific Instruments*: 71(7), 2669–2676. 2000.

[6] Masroor I, Ghazanfar H. Michelson interferometer for precision angle measurement. *Applied Optics*: 38, 113-120. 1999.

[7] Cai M, et al. Event2Audio: Event-Based Optical Vibration Sensing. *arXiv*: 2025.

[8] Sheinin M, Chan D, O'Toole M, and Narasimhan SG. Dualshutter optical vibration sensing. *Proceedings of the IEEE/CVF Conference on Computer Vision and Pattern Recognition*: 16324-16333. 2022.

[9] Hasheminejad N, Vuye C, Van den Bergh W, Dirckx J, Vanlanduit S. A comparative study of laser Doppler vibrometers for vibration measurements on pavement materials. *Infrastructures*: 47. 2018.

[10] Gallego G, Delbruck T, Orchard G, Bartolozzi C, Taba B, Censi A, Leutenegger S, Davison AJ, Conradt J, Daniilidis K, and Scaramuzza D. Event-based vision: A survey. *IEEE Transactions on Pattern Analysis and Machine Intelligence*: 154-180. 2022.

[11] Fu M, Dornseiff J, Barth V, and Scheer E. Time-averaged interference fringe analysis: A quantitative study of nanomembrane vibration dynamics. *Sensors and Actuators A: Physical*: 116172. 2025.

[12] Teich MC and Saleh B. Fundamentals of photonics. *Vol. 2*. New Jersey: Wiley. 2007.

[13] Bardow et al. Simultaneous Optical Flow and Intensity Estimation From an Event Camera. *IEEE XPlore*. 2016.

[14] Maciejewski MW, Qui HZ, Rujan I, Mobli M, Hoch JC. Nonuniform sampling and spectral aliasing. *J Magn Reson*: 199(1), 88-93. 2009.

[15] Oppenheim AV, Schafer RW. Discrete-Time Signal Processing. 3rd ed. *Prentice Hall*. 2009.

[16] Van Loan C. Computational frameworks for the fast Fourier transform. *Society for Industrial and Applied Mathematics*. 1992.

Appendix A

Expected Acoustic Vibration Amplitude

The amplitude of surface vibrations depends on the material properties—specifically its mass density, thickness, and stiffness—as well as the characteristics of the acoustic excitation.

Interference Intensity Relationship

The maximum interference intensity $I_{\max}$ occurs when the phase difference $\Delta\phi = 0$:

$$I_{\max} = 4I_0 \cos^2(0) = 4I_0$$

where I_0 is the reference intensity from one interferometer arm. For a phase change of one radian:

$$I = I_0 + I_0 + 2\sqrt{I_0^2}\cos(1) \approx 2I_0 + 2I_0(0.5403) \approx 3.0806I_0$$

Hence, the change in intensity relative to the maximum is:

$$4I_0 - 3.0806I_0 = 0.9194I_0$$

corresponding to approximately a 23% change in intensity.

Vibration Model

To model the vibration amplitude induced by an acoustic signal, the vibrating surface can be approximated as a driven damped harmonic oscillator governed by:

$$m\frac{d^2x}{dt^2} + b\frac{dx}{dt} + kx = F_0 e^{i\omega t}$$

where:

- m = effective mass of the vibrating surface (kg),
- b = damping coefficient (kg/s),
- k = stiffness or spring constant (N/m),
- F_0 = amplitude of the external driving force (N),
- ω = angular frequency of the driving acoustic wave (rad/s),
- $x(t)$ = displacement of the surface (m).

Solution

The steady-state solution is given by:

$$x(t) = Ae^{i(\omega t - \theta)}$$

where the vibration amplitude A and phase lag θ are given by:

$$A = \frac{F_0}{\sqrt{(k - m\omega^2)^2 + (b\omega)^2}}$$

$$\theta = \tan^{-1}\left(\frac{b\omega}{k - m\omega^2}\right)$$

Interpretation

The goal is to identify a maximum allowable vibration amplitude A such that the induced surface displacement does not exceed one full interference fringe (approximately 300 nm), while remaining above the system's minimum detectable displacement threshold. By selecting appropriate material parameters—mass m, stiffness k, and damping b—and using the above expression for A, one can determine whether the vibration response will remain within the desired operating range.